Inorganic Chemistry

Article

pubs.acs.org/IC

# Nonprecious Metal Catalysts for Fuel Cell Applications: Electrochemical Dioxygen Activation by a Series of First Row Transition Metal Tris(2-pyridylmethyl)amine Complexes

Ashleigh L. Ward,[†] Lior Elbaz,[‡] John B. Kerr,[§] and John Arnold*[,†]

[†]Department of Chemistry, University of California, Berkeley, California 94720, United States

[‡]Materials Physics & Applications Division, Los Alamos National Laboratory, Los Alamos, New Mexico 87545, United States

[§]Environmental Energy Technologies Division, Lawrence Berkeley National Laboratory, Berkeley, California 94720, United States

Supporting Information

**ABSTRACT:** A series of divalent first row triflate complexes supported by the ligand tris(2-pyridylmethyl)amine (TPA) have been investigated as oxygen reduction catalysts for fuel cell applications. $[(TPA)M^{2+}]^{n+}$ (M = Mn, Fe, Co, Ni, and Cu) derivatives were synthesized and characterized by X-ray crystallography, cyclic voltammetry, NMR spectroscopy, magnetic susceptibility, IR spectroscopy, and conductance measurements. The stoichiometric and electrochemical $O_2$ reactivities of the series were examined. Rotating-ring disk electrode (RRDE) voltammetry was used to examine the catalytic activity of the complexes on a carbon support in acidic media, emulating fuel cell performance. The iron complex displayed a selectivity of 89% for four-electron conversion and demonstrated the fastest reaction kinetics, as determined by a kinetic current of 7.6 mA. Additionally, the Mn, Co, and Cu complexes all showed selective four-electron oxygen reduction (<28% $H_2O_2$) at onset potentials (~0.44 V vs RHE) comparable to state of the art molecular catalysts, while being straightforward to access synthetically and derived from nonprecious metals.

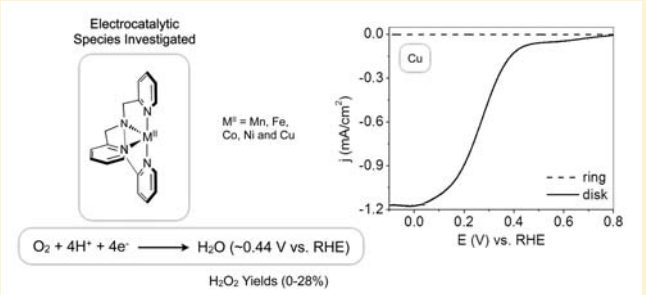


## INTRODUCTION

Determining the factors that govern the activation of dioxygen by transition metal coordination compounds is of fundamental importance to a wide variety of synthetic and biological transformations.[1−10] One application of particular interest lies in energy conversion technologies, where the electrochemical four-electron reduction of dioxygen to water (eq 1) is utilized

$$O_2 + 4H^+ + 4e^- \rightarrow 2H_2O \quad (1.23\ \text{V vs SHE}) \qquad (1)$$

in proton exchange membrane fuel cells (PEMFC).[11−15] While thermodynamically very favorable, the oxygen reduction reaction (ORR) is currently mediated by platinum-based electrocatalysts, whose high cost, scarcity, and kinetic inefficiencies have hindered fuel cell commercialization.[11,12,16,17] It is therefore desirable to study nonprecious metal catalysts capable of four-proton and four-electron ORR via a selective and complete pathway.

Traditionally, solid-state materials have been incorporated as electrocatalysts in PEMFCs.[12,17−20] However, the use of transition metal coordination compounds as ORR catalysts has gained interest in recent years.[13,15,21,22] This is due to the ability to accurately characterize the catalytic active site and tune reactivity. The design of such molecular systems has taken a biomimetic approach, seeking to model the active sites of oxygen binding and activating enzymes, such as the P450 family of proteins and blue-copper laccases.[4,23−25] As such, great attention has been given to complexes that contain iron and copper: the two transition metal ions most often utilized in nature for manipulating oxygen.

However, oxygen activation and binding have been demonstrated with all of the late first row transition metals, employing a diverse set of ligand systems. The oxygenation chemistry of both iron and cobalt has been heavily focused on porphyrins[4,23,26] and corroles,[24] where catalytic reduction has been observed. Additionally, a propensity for four-electron reduction has been recently demonstrated with both a monomeric manganese complex[27] and a nickel bis-(diphosphine) complex.[28] The study of copper $O_2$ activation chemistry has been tailored to emulate copper laccases, often utilizing tris(2-pyridylmethyl)amine (TPA; also abbreviated TMPA or Npy3) analogues (Figure 1a) as molecular mimics.[10,12,25,29,30] Clearly, many first row coordination compounds exhibit the reactivity desired for employing a molecular catalyst in fuel cells. However, given the diversity in coordination environments, extracting a coherent design strategy with regard to the metal center remains difficult.

Iron and copper derivatives of TPA (Figure 1b and c) have been studied as $O_2$ activation catalysts for some time.[10,25,37−40]

**Received:** December 14, 2011
**Published:** March 29, 2012

   dx.doi.org/10.1021/ic2026957 | Inorg. Chem. 2012, 51, 4694−4706

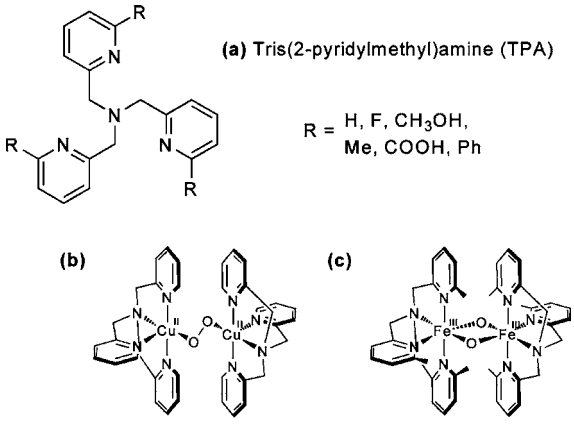


**Figure 1.** Ligand of interest, TPA, and significant $O_2$ adducts. (a) Tris(2-pyridylmethyl)amine (TPA) ligand and various derivatives.[31−36] (b) $[Cu_2(\mu\text{-}O_2)(TPA)_2](PF_6)_2$.[30] (c) $[Fe_2(\mu\text{-}O)_2(5\text{-Me-TPA})_2](ClO_4)_2$.[37]

There is also recent literature precident for electrocatalytic $O_2$ reduction by a copper(II) complex immobilized on an electrode surface.[41] However, the dioxygen reactivity of other late transition metal complexes of this ligand has not been reported. Recently, a related copper TPA complex has been employed as an ORR electrocatalyst.[42] However, the electrocatalytic oxygen reduction proficiency of a series of TPA metal complexes has not been examined. Given our interest in determining the best method for selecting a molecular species to employ as a fuel cell catalyst, the effect of varying the metal center in a ligand system known to be capable of ORR was studied. A series of first row triflate (OTf) TPA homologues were prepared. The dioxygen reactivity—both stoichiometric and electrochemical—of the compounds is presented. Additionally, the complexes were examined using traditional evaluation methods for ORR electrocatalysts, and their performance as catalysts on a carbon support in Nafion is described.

## RESULTS AND DISCUSSION

**Synthesis and Structural Properties.** The advantages of homogeneous catalysis over heterogeneous catalysis are that the catalytic species of interest, as well as reactive intermediates, are readily characterized via classical methods.[43,44] In turn, this allows for straightforward deciphering of the catalytic mechanism and subsequent catalyst tuning. The aim of this work is to utilize a molecular catalyst in a traditionally heterogeneous system. This will provide a means for relating molecular behavior to the performance seen in the applied system by first accurately and thoroughly characterizing the molecular species of interest.

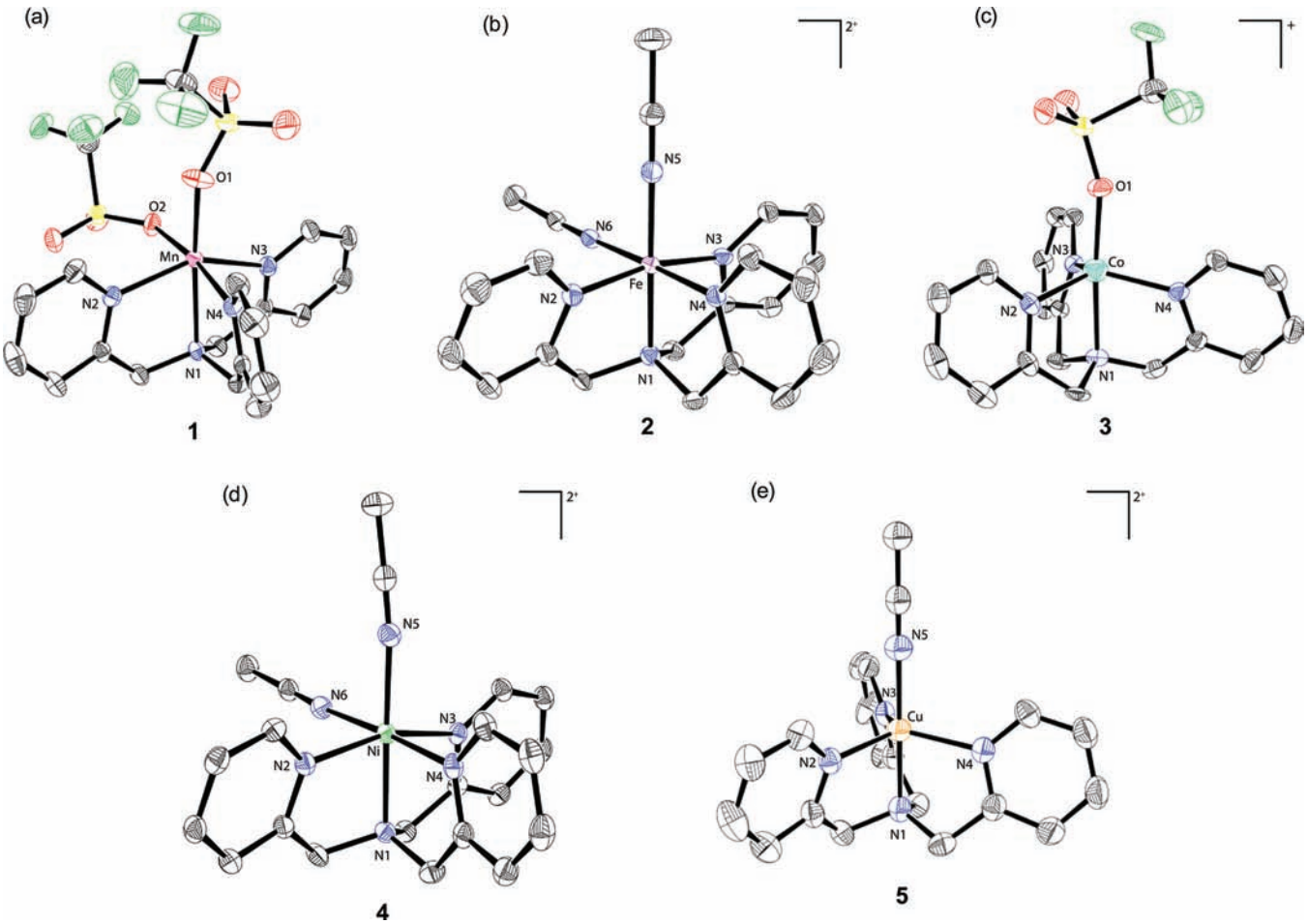


**Figure 2.** Crystal structures of complexes **1**−**5**: (a) $(TPA)Mn(OTf)_2$ (**1**), (b) $[(TPA)Fe(MeCN)_2]^{2+}$ (**2**), (c) $[(TPA)Co(OTf)]^{+}$ (**3**), (d) $[(TPA)Ni(MeCN)_2]^{2+}$ (**4**), and (e) $[(TPA)Cu(MeCN)]^{2+}$ (**5**), respectively. Note: the secondary coordination sphere has been eliminated for clarity.


dx.doi.org/10.1021/ic2026957 | Inorg. Chem. 2012, 51, 4694−4706

**Table 1. Selected Bond Lengths (Å) and Angles (deg) for Complexes 1−5**

| compd | 1 | 2[a] | 3 | 4 | 5[b] |
|---|---|---|---|---|---|
| | | Bond Lengths (Å) | | | |
| M−N1 | 2.289(2) | 1.978(3) | 2.162(5) | 2.090(2) | 2.007(7) |
| M−N2 | 2.235(2) | 1.962(3) | 2.037(5) | 2.071(2) | 2.037(3) |
| M−N3 | 2.243(2) | 1.959(3) | 2.039(5) | 2.069(2) | |
| M−N4 | 2.252(1) | 1.953(3) | 2.041(5) | 2.071(2) | |
| M−N5 | | 1.933(3) | | 2.034(2) | 1.949(7) |
| M−N6 | | 1.947(3) | | 2.126(2) | |
| M−O1 | 2.114(1) | | 2.016(4) | | |
| M−O2 | 2.169(1) | | | | |
| | | Bond Angles (deg) | | | |
| N1−M−N2 | 76.13(6) | 83.6(1) | 79.7(2) | 81.49(7) | 82.7(2) |
| N1−M−N3 | 74.19(6) | 83.2(1) | 79.0(2) | 80.96(7) | |
| N1−M−N4 | 77.01(6) | 85.7(1) | 79.0(2) | 82.96(7) | |
| N2−M−N4 | 81.31(6) | 91.6(1) | 118.2(2) | 88.58(7) | 120.0 |
| N1−M−N5 | | 178.6(1) | | 178.03(7) | 180.0 |
| N1−M−O1 | 166.52(6) | | 175.5(2) | | |

[a]Select bond lengths (Å) and angles (deg) for **2** are appended from ref 49. [b]Complex **5** possesses a unit cell comprised of three highly symmetric $^1/_3$ fragments of the molecule. Each possesses a $C_3$ element of symmetry that generates the rest of the molecule. As a result, the M−N1, M−N2, and M−N5 distances and N1−M−N2 angle are presented as an average of the three.

As an initial proof of concept, a simple molecular system capable of ORR and compatible with a fuel cell environment was selected for study. The TPA scaffold has been shown to support complexes capable of oxygen activation.[25,29,37,39,45] Triflate anions are weakly coordinating, providing the possibility for open coordination sites, and they closely resemble the terminal perfluoroalkylsulfonate anions present in the Nafion polymer electrolyte membrane.[46,47] Given their compatibility with our design criteria, divalent manganese, iron, nickel, and copper bis(triflate) complexes of TPA were synthesized by reaction of the corresponding $M^{2+}$ triflate salt with the ligand in acetonitrile. The cobalt(II) derivative was synthesized via salt metathesis between $Co(TPA)Cl_2$[48] and Ag(OTf). Filtration of the reaction mixtures followed by recrystallization from MeCN afforded the desired $(TPA)Mn(OTf)_2$ (**1**), $[(TPA)Fe(MeCN)_2](OTf)_2$[49] (**2**), $[(TPA)Co(OTf)](OTf)$ (**3**), $[(TPA)Ni(MeCN)_2](OTf)_2$ (**4**), and $[(TPA)Cu(MeCN)](OTf)_2\cdot(MeCN)$ (**5**) in good to excellent yields (78−96%) (Figure 2).

$(TPA)Mn(OTf)_2$ is unusual in that most Mn(TPA) complexes found in the literature are bimetallic catalase mimics,[50,51] while **1** (Figure 2a) is monomeric. The relatedness of oxygenase chemistry to oxygen reduction, as well as recent literature precedent for oxygen reduction by a monometallic Mn complex containing nitrogen donors,[27] lend support to utilizing **1** as an ORR catalyst. As with all the complexes in the $M^{2+}$ triflate series **1**−**5** in the solid-state, the TPA ligand is coordinated in a tripodal tetradentate fashion in **1**. The geometry about the manganese center in **1** is a distorted octahedron, with two triflate anions occupying the remaining coordination sites, and it represents the only neutral complex in **1**−**5**. The TPA ligand is folded away from the steric and electronic bulk of the coordinated triflate ions, as evidenced by the average $N_{pyridine}-Mn-N_{amine}$ angle deviation from the mean square plane of the octahedron of 14.22(6)°.

The $Mn-N_{amine}$ distance (Table 1) of 2.289(2) Å is similar to that of the closely related manganese(II) TPA dichloride,[52] which is also a neutral octahedral complex. The three pyridyl nitrogens are bound to the manganese center at similar distances, 2.235(2), 2.243(2), and 2.252(1) Å, respectively, with the nitrogen trans to the triflate ligand having the longest bond length, as expected due to the higher trans effect of the anionic triflate. The triflate distances concur with this assessment, with one anion being labile, allowing for an available coordination site for catalysis. The triflate trans to the pyridyl nitrogen has a longer distance (2.169(1) Å) than that of the triflate trans to the amine (2.114(1) Å), which lacks a $\pi$ system capable of an additional $\pi$ trans effect.

Iron(II) TPA derivatives have been studied extensively as bioinspired nonheme catalysts for oxygen activation and transfer reactions.[40,53] The iron derivative **2** (Figure 2b) is dicationic and adopts an octahedral coordination mode, similar to other iron oxygen activation catalysts. In addition to the $\eta_4$-TPA, two acetonitrile molecules are bound to the Fe(II) center in **2** and two triflate anions are present in the secondary coordination sphere.

The $Fe-N_{amine}$ distance (1.978(3) Å) is the longest of the nitrogens bound to the metal center, as is expected given its lack of ability for $\pi$ donation. The $Fe-N_{pyridine}$ bonds are quite similar (1.962(3), 1.959(3), and 1.953(3) Å, respectively), with the nitrogen trans to the coordinated acetonitrile having the shortest distance, presumably due to trans effects. While labile enough to allow for substrate binding, the acetonitrile distances represent the shortest for the iron derivative and are likely a consequence of the favorability of enforcing a low-spin state. Consistent with other iron TPA complexes, the stronger field acetonitriles bound in **2** allow for a low-spin 18-electron complex, whereas neutral derivatives with anions directly bound to the iron center yield high-spin complexes.

The cobalt derivative **3** (Figure 2c) exhibits a trigonal bipyramidal geometry that is unusual for an oxygen reduction catalyst. Cobalt ORR catalysts typically are square pyramidal.[23,54] In complex **3**, TPA is again bound $\eta_4$, with one triflate molecule bound directly to the metal center, giving a 17-electron complex. An additional triflate anion is present in the secondary coordination sphere, making **3** monocationic. In the case of **3**, the pyridyl arms are coordinated in a roughly symmetric fashion about the cobalt center. There is a slight distortion away from the coordinated triflate ion, as evidenced by the N2−Co−N4 angle of 118.2(2)° (Table 1). This is also


dx.doi.org/10.1021/ic2026957 | Inorg. Chem. 2012, 51, 4694−4706

**Table 2. Crystal and Refinement Data for Complexes 1−5**

| | 1 | 2[a] | 3 | 4 | 5 |
|---|---|---|---|---|---|
| empirical formula | $C_{20}H_{18}F_6MnN_4O_6S_2$ | $C_{24}H_{24}F_6FeN_6O_6\ S_2$ | $C_{20}H_{18}CoF_6N_4O_6S_2$ | $C_{24}H_{24}F_6N_6NiO_6\ S_2$ | $C_{24}H_{24}CuF_6N_6O_6S_2$ |
| molecular weight | 643.44 | 767.52 | 647.45 | 729.32 | 734.14 |
| temp (K) | 130(2) | 173(2) | 100(2) | 100(2) | 121(2) |
| cryst syst | monoclinic | monoclinic | orthorhombic | monoclinic | trigonal |
| space group | $P2_1/c$ | $P2_1/n$ | $Pbca$ | $P2_1/n$ | $P3c1$ |
| $a$ (Å) | 17.689(3) | 12.418(2) | 14.6412(14) | 8.7494(4) | 12.502(3) |
| $b$ (Å) | 9.7630(15) | 16.192(4) | 12.2822(11) | 9.2921(4) | 12.502(3) |
| $c$ (Å) | 16.092(2) | 15.855(2) | 28.154(3) | 36.9208(17) | 33.347(9) |
| $\alpha$ (deg) | 90 | 90 | 90 | 90 | 90 |
| $\beta$ (deg) | 113.203(2) | 92.09(2) | 90 | 95.994(2) | 90 |
| $\gamma$ (deg) | 90 | 90 | 90 | 90 | 120 |
| vol (Å$^3$) | 2554.2(7) | 3585.8(10) | 5062.8(8) | 2985.3(2) | 4514(2) |
| $Z$ | 4 | 4 | 8 | 4 | 6 |
| $\lambda$ (Å) | 0.71073 | 0.71073 | 1.5418 | 1.54178 | 0.71073 |
| $\mu$ (mm$^{-1}$) | 0.769 | 0.692 | 0.932 | 3.045 | 0.951 |
| no. rflns measd | 44420 | 6846 | 122621 | 19654 | 48764 |
| no. indep reflns | 4685 | 5616 | 4646 | 5303 | 5509 |
| $R_{int}$ | 0.0493 | 0.0389 | 0.0351 | 0.0188 | 0.0471 |
| restr/param | 0/352 | 0/433 | 0/352 | 0/408 | 1/422 |
| $R_1$, $wR_2$ | 0.0262, | 0.0441, | 0.0253, | 0.0374, | 0.0398, |
| $[I > 2\sigma(I)]$ | 0.0603 | 0.1044 | 0.0620 | 0.0932 | 0.0860 |
| $R_1$ (all data) | 0.0402 | 0.0657 | 0.0284 | 0.0404 | 0.0518 |
| GOF | 0.916 | 1.060 | 1.048 | 1.115 | 1.057 |

[a]For completeness, crystal and refinement data for **2** are appended from ref 49.

apparent in the $\tau$ value,[55] a common measure of the distortion from the idealized trigonal bipyriamidal geomoetry, of $\tau = 0.95$.

Complex **3** is one of only four 5-coordinate divalent cobalt TPA species, most of which have been studied for their magnetic properties.[56,57] The bis(triflate) derivative structurally resembles previously reported $[Co(TPA)Cl]^+$ cations.[48,58] The $Co-N_{amine}$ distance is the longest of the coordinated nitrogens at 2.162(5) Å, and the $Co-N_{pyridine}$ distances are all identical within error (2.039(5) Å). This is not the case with the manganese and iron derivatives and is presumably due to the lack of a significant trans effect from a sixth ligand coordinated trans to a pyridyl nitrogen. The $Co-O_{OTf}$ distance is 2.016 Å. The values for reported chloride derivatives are significantly longer, displaying very weak interactions (2.2759(6) and 2.279(2) Å, respectively).[49,58] This can be attributed to a better hard−hard pairing, as well as the presence of a delocalized $\pi$ system present in the triflate ligand.

While not as common as the other first row metals presented in this work, there is some precedent for oxygen activation at nickel, although typically with softer ligands such as phosphines.[28] Much like iron complex **2**, the nickel TPA triflate derivative **4** (Figure 2d) possesses a roughly octahedral coordination environment, with two acetonitriles bound to the metal center in addition to the $\eta_4$-TPA. Two triflate anions are present in the outer coordination sphere, making the complex dicationic.

Species **4** is somewhat unusual in that it is a 20-electron complex. While not unprecedented for nickel(II) derivatives,[58] breaking the 18-electron rule create a coordinatively saturated nickel center in **4** that makes substrate binding difficult. The electronic consequences of coordinating a sixth ligand are evidenced in the structural data. The $Ni-N_{amine}$ distance is similar to those of other divalent nickel TPA complexes at 2.090(2) Å.[36,59] Interestingly, however, a trans effects seen in the manganese and iron derivatives **1** and **2** are absent in **4**, with the pyridyl nitrogens all possessing, within error, identical bond lengths of 2.070(2) Å. The lack of a trans effect is likely due to the labile nature of the second acetonitrile ligand, which if bound more strongly would inherently affect the bonding of the pyridyl nitrogen trans to it. This lability is demonstrated by the fact that although the pyridyl nitrogens lack any evidence of the trans effect, the two coordinated acetonitriles display a dramatic difference in bond lengths (2.034(2) vs 2.126(2) Å), with the weaker coordination again occurring trans to the pyridyl nitrogen of TPA. This weak coordination of the sixth ligand is seen in $[Ni(Ph_1TPA)(CH_3CN)_2](ClO_4)_2$[60] and $[Ni(Me_3TPA)(CH_3CN)_2](ClO_4)_2$,[61] both of which are dicationic 20-electron nickel complexes.

The final complex in the triflate TPA series is the dicationic copper complex **5** (Figure 2e). Copper derivatives of the TPA ligand have been studied for some time as blue copper protein mimics for oxygen activation and electron transfer reactions.[10,62] The structural characteristics of **5** are similar to those of several isostructural dications present in the literature.[31,63,64] Much like the cobalt derivative **3**, **5** employs a trigonal bipyramidal geometry ($\tau = 1.00$), with $\eta_4$-TPA bound in a tripodal fashion, and an acetonitrile molecule occupying the remaining coordination site. Additionally, there are two triflate anions in the secondary coordination sphere.

Complex **5** is highly symmetric, with one-third of the molecule sitting on a $C_3$ element of symmetry that generates the rest (Table 2 contains relevant crystallographic data). Three of these symmetric one thirds are comprised in the asymmetric unit, and the $Cu-N_{pyridine}$ distances given are an average of the three. Similar to the cases of several other copper TPA derivatives,[31,65] the $Cu-N_{amine}$ distance in **5** is 2.007(7) Å. Moving from **1** to **5**, this $M-N_{amine}$ distance consistently decreases, apart from the iron complex **2**, which displays the shortest distance. This trend is in agreement with the Shannon


dx.doi.org/10.1021/ic2026957 | Inorg. Chem. 2012, 51, 4694−4706

ionic radii trends, as well as those expected given the extra stabilization afforded via low-spin versus high-spin iron(II).[65]

The $Cu-N_{pyridine}$ distances are all equivalent (2.037(3) Å), with the N1−Cu−N5 line comprising a $C_3$ axis. In turn, each $N_{pyridine}-Cu-N_{pyridine}$ angle is 120°, generated via crystallographic symmetry. Additionally, as in complexes **2** and **4**, the $Cu-N_{MeCN}$ distance of 1.949(7) Å represents the shortest of the bound nitrogens and is likely due to the better hard−hard pairing of the N-donor with the metal center.

Across the series **1**−**5**, and closely related to the manner in which $O_2$ is bound, each complex displays a geometry that is related to the intrinsic preference that each metal in a particular oxidation state possesses. High spin $d^5$ complexes adopt a tetrahedral geometry; however, in **1**, coordination of the triflate ions yields a 17-electron complex. This is presumably more favorable than the 13-electron complex that would arise from a tetrahedral Mn(TPA) dication. As seen in **2**, strong field ligands tend to form low-spin $Fe^{2+}$ complexes that coordinate octahedrally to yield a closed shell.

The case of **4** is somewhat unusual in that adoption of an octahedral coordination environment affords a 20-electron complex. A $d^8$ metal is typically expected to employ a coordination number of either 4 or 5, giving rise to a low-spin 16- or 18-electron complex, respectively. However, due to electronegativity trends, the d orbitals of late transition metals are often low enough in energy to accommodate electrons in the antibonding $e_g$* level. This is true for **4** and other TPA nickel adducts.[60,66]

Cobalt(II) and copper(II) each possess 7 and 9 d electrons, respectively, and in the case of **3** and **5** coordinate in a trigonal bipyramidal fashion. Complex **3** is one of the only pentacoordinate cobalt(II) complexes, two of which are other TPA derivatives, with the vast majority being either square pyramidal or octahedral.[57,67] A trigonal bipyramidal coordination mode is typical for copper(II) species, and in addition to **5**, it is seen extensively in copper TPA chemistry.[29,39] As with $Ni^{2+}$, the d orbitals are low enough in energy to accommodate electrons in antibonding orbitals. Decoordination of the ancillary ligand would give rise to a four-coordinate species capable of binding substrate via the respective d orbitals.

**Physical Properties.** Using the Evans' NMR method,[68] the magnetic susceptibility of each complex was determined in solution. Except for **3**, all complexes displayed the spin states afforded via a simple crystal field splitting analysis. The colorless manganese complex **1** gave a $\mu_{eff}$ of 5.9(1) $\mu_B$, corresponding to $S = {}^5/_2$, as expected for high-spin $Mn^{2+}$. Iron complex **2** is red, as is typical of many low-spin $Fe^{2+}$ complexes, and is diamagnetic.

The magnetism of complex **3** is different than predicted using a strict crystal field splitting analysis for cobalt(II) in a trigonal bipyriamidal geometry. One unpaired electron is expected in the e′ level. However, complex **3** gave a $\mu_{eff}$ of 4.2(1) $\mu_B$, corresponding to $S = {}^3/_2$. A likely explanation of this behavior lies with the ancillary ligand. The weak field nature of the triflate anion destabilizes its interaction with the metal center, causing the energy splitting to decrease, thus bringing the a1′ orbital to a comparable level with the e′ orbitals. This molecular orbital picture yields three unpaired spins and is not unprecedented for cobalt(II) compounds in this geometry.[69,70]

The nickel derivative **4** displays a distorted octahedral geometry, and as such the measured $\mu_{eff}$ of 2.9(1) $\mu_B$, corresponding to $S = 1$, is consistent with the expected half-filled $e_g$* level. Interestingly, this indicates that while the second coordinated acetonitrile is quite labile, the formation of 20-electron complex **4** is not purely a crystal packing effect, as evidenced by the solution data. Copper complex **5** gave a $\mu_{eff}$ of 1.5(1) $\mu_B$, corresponding to $S = {}^1/_2$, which is coherent, as a $d^9$ metal possesses one unpaired spin no matter the coordination number.

Variable concentration conductance measurements were taken for each complex in the same solvent used to crystallize them: acetonitrile. Onsager plots of complexes **1**−**5** (Figure 3)

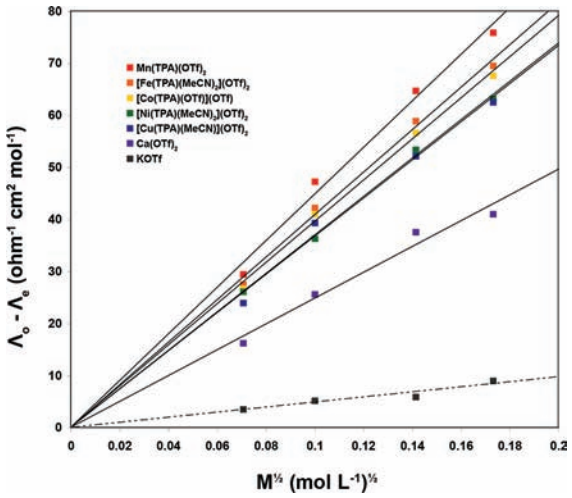


**Figure 3.** Onsager plots for complexes **1**−**5**, indicating 2:1 (—) and 1:1 (—···—) electrolytes, respectively.

were constructed and compared to electrolyte standards of both 1:1 (KOTf) and 2:1 ($Ca(OTf)_2$) triflate salts. In contrast to the structural trends observed in the solid-state, all compounds are 2:1 electrolytes in acetonitrile, meaning that the apparent preference for coordination of triflate versus acetonitrile is a solid-state packing effect. The magnetism data described above was also taken in acetonitrile, indicating that the geometry, and therefore coordination number, of each compound remains the same in solution. In the **1**−**5** series, acetonitrile has a high enough dielectric constant to support solvent separated ion pairs, and it also appears to coordinate to the manganese and cobalt complexes in place of triflate ions.

The $^1$H NMR data is consistent with the highly paramagnetic nature of the TPA triflate series **1**−**5**. The copper, nickel, and manganese complexes all yield highly paramagnetically shifted, as well as broadened, spectra. The cobalt complex gives a spectrum that is quite shifted but also sharp, and the iron complex yields resonances in the diamagnetic region (Figure 4). In complexes **2** and **3**, signals corresponding to each of the pyridyl protons, as well as the methylene linker, are easily discernible. The $^1$H NMR spectra of both **2** and **3** possess five proton resonances, suggesting that the complexes have 3-fold symmetry with regard to the TPA ligand. On the time scale of the NMR experiment, there is an exchange between the pyridyl arms that averages their environments in solution, as has been observed with a related copper(I) TPA complex.[71]

The spectrum of iron complex **2** is in the diamagnetic region, with the methylene protons giving a broad singlet at 6.88 ppm. The pyridyl proton resonances are shifted in accordance with their proximity to the metal center. The $\alpha$ proton, closest to the iron(II) center, is shifted the furthest downfield at 11.82 ppm (s), the two $\beta$ protons give indiscernible overlapping singlets at


dx.doi.org/10.1021/ic2026957 | Inorg. Chem. 2012, 51, 4694−4706

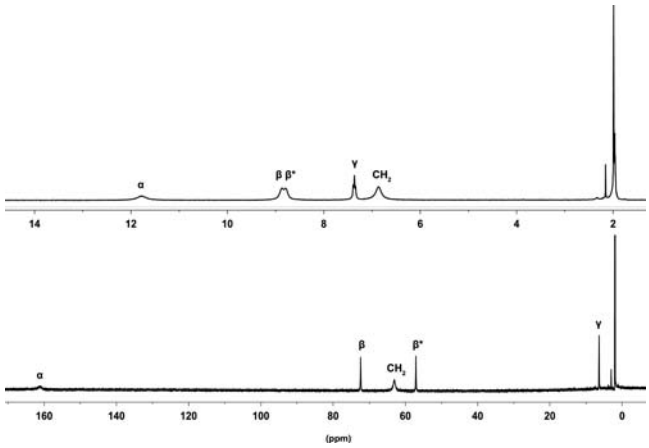


**Figure 4.** $^{1}$H NMR spectra of **2** (top) and **3** (bottom), illustrating the five resonances that correspond to the protons of the pyridyl arms of the ligand, which are all equivalent in solution.

8.88 and 8.78 ppm, respectively, and the $\gamma$ proton resonates at 7.32 ppm (s).

Likewise for cobalt complex **3**, there is fluxionality apparent in solution, as indicated by the presence of only five signals. On the basis of the relative ratios of the resonances, the peak at 63.08 ppm (s) is assigned to the methylene protons. The peak furthest downfield at 161.40 ppm (s) is assigned to the $\alpha$ pyridine proton. This is nearly analogous to the assignments made in **2** and is consistent with the proximity of each proton to the paramagnetic Co(II) center. The $\beta$ protons appear at 72.36 (s) and 57.04 ppm (s) respectively, and the $\gamma$ proton resonates furthest upfield at 6.33 ppm (s).

Dynamic solution behavior is also evident in the $^{19}$F NMR of complexes **1**−**5**, and concurs with the dicationic assignment made for the compounds via conductivity measurements. All five complexes display a single resonance, indicating an exchange between the two triflate anions present in each. Free triflate has an approximate fluorine resonance at −78 ppm.[72,73] The fluorine resonances for the iron (−77.96 ppm), cobalt (−77.09 ppm), nickel (77.91 ppm), and copper (−78.25 ppm) complexes all indicate that neither triflate ion is bound to the metal center in solution. The resonance present in the manganese spectrum at −52.80 ppm seems to indicate an interaction with the metal center, but the highly paramagnetic nature of the complex and broadened signal could also cause the apparent shift.

The lability of the acetonitriles bound to complexes **2**, **4**, and **5** seen in the structural data is also evidenced in the solid-state IR. Free acetonitrile gives two stretches reported at 2292 and 2253 cm$^{-1}$.[74] As such, the iron complex **2** is expected to have four CN stretches, given the two acetonitriles bound in the crystal structure, but it appears that the solvent is lost too quickly, and the corresponding IR stretches are unobserved. Additionally, the diamond anvil cell used for the IR measurements has a broad absorption around 2000 cm$^{-1}$ that limits the detection.[75] Therefore, given the weak nature of the CN stretches observed, this in combination with the rapid loss of solvent could account for the lack of signals seen for **2**. For the nickel complex **4**, which has two acetonitriles bound in the solid-state, there are four signals at 2324, 2307, 2295, and 2281 cm$^{-1}$. This is expected from the two signals that are attributed to two different IR active modes for free acetonitrile. Additionally, the copper complex **5** possesses two CN stretches at 2330 and 2299 cm$^{-1}$, respectively, consistent with the one acetonitrile bound in the crystal structure.

**Stoichiometric Reactivity with $O_2$.** In designing an ORR catalyst, it remains important to balance the need to not only bind and activate the $O_2$ bond, but in turn avoid the formation of a stable metal-oxo with the catalyst, as this would prevent further reduction and protonation. Thus, the reactivity of complexes **1**−**5** toward $O_2$ in the absence of protons and electrons was examined. Each divalent complex was reacted with a stoichiometric amount of dioxygen under the same conditions under which electrochemical measurements were conducted.

Manganese complexes have not been as extensively studied for their oxygen reactivity as other first row derivatives. This is evidenced by the strikingly low number of structurally characterized Mn-dioxygen adducts.[76] Two notable examples are a manganese porphyrin and a Tp complex.[77,78] Both bind $O_2$ in a side-on fashion and are thermally unstable at temperatures above −78 °C. However, an $O_2$ adduct is not observed with the TPA complex **1**, due most likely to the fact that binding is labile at ambient temperature. Additionally, some manganese complexes, such as Mn salphen, react with oxygen to form highly stable $\mu$-oxo dimers.[77] Yet, potentially due to the starkly different coordination environment, this behavior is not observed for complex **1**, as no Mn-oxo products were isolated from its reaction with dioxygen.

When trying to reduce oxygen to water using an iron catalyst, side reactions leading to the formation of thermodynamically stable iron-oxos are problematic. Complex **2** proves to have such behavior. Reaction of **2** with dioxygen followed by filtration and recrystallization from acetonitrile yielded $[(TPA)_2Fe_2(\mu\text{-}O)(OTf)_2](OTf)_2$ (**6**) in 66% yield. The mechanism for the formation of **6** is likely similar to those reported for iron porphyrin systems.[53] The solid-state structural characteristics of **6** (Figure 5) are similar to those presented for a series of related chloride derivatives.[34] The Fe1−O−Fe2 angle is nearly linear (174.6(2)°). Two triflate molecules are directly bound to the dimer, with two present in the outer coordination sphere. One coordinated triflate molecule is disordered and was modeled accordingly (only one occupancy is depicted for clarity). The magnetic susceptibility is 3.2(1) $\mu_B$ for **6**, corresponding to high-spin iron(III) centers which are antiferromagnetically coupled, similar to other oxo dimers of iron.[79]

Divalent cobalt complexes such as cobalt salen are well-known for their ability to reversibly bind $O_2$. Additionally, the propensity of cobalt complexes, such as cobalt porphyrins, to reduce oxygen to water has been examined.[23] Nonetheless, we are unaware of reports of cobalt TPA complexes being investigated for such reactivity. Neither oxygen binding nor oxygen activation under ambient conditions was observed with complex **3**. As with the manganese complex **1**, it is possible that a facile exchange with $O_2$ as a ligand is occurring but that it is too weak to observe at room temperature.

Reaction of the nickel and copper complexes **4** and **5** with oxygen returned only starting material. This is as expected for these metals in their divalent states. Nickel(I) complexes have been shown to react with dioxygen;[80] however, the only reactivity toward oxygen seen with a nickel(II) species was with the diphosphine complex mentioned earlier.[28] It is thus not surprising that complex **4** showed no reactivity toward $O_2$. Similarly, copper(I) complexes are known to react readily with oxygen, much like the blue copper proteins. Copper TPA


dx.doi.org/10.1021/ic2026957 | Inorg. Chem. 2012, 51, 4694−4706

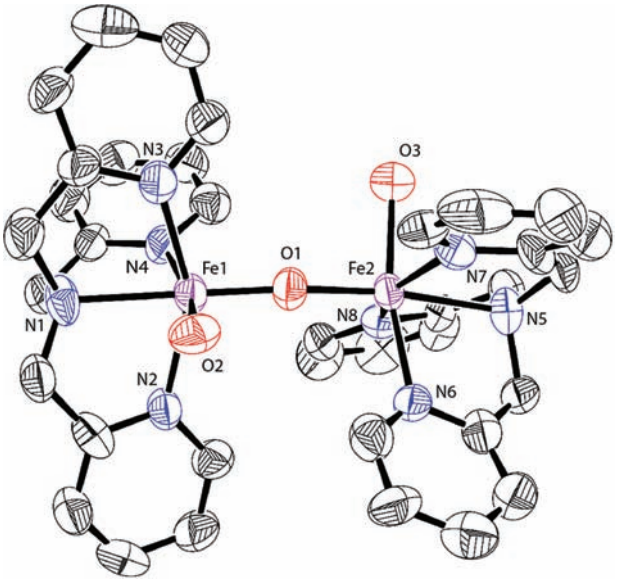


**Figure 5.** $\mu$-oxo iron dimer **6**. OTf anions have been truncated to coordinated oxygens O2 and O3 for clarity. Select bond lengths (Å) and angles (deg): Fe1−O1, 1.766(3); Fe2−O1, 1.814(3); Fe1−O2, 2.124(4); Fe2−O3, 2.127(4); Fe1−N1, 2.219(4); Fe1−N2, 2.122(4); Fe1−N3, 2.099(5); Fe1−N4, 2.157(5); Fe2−N5, 2.229(4); Fe2−N6, 2.147(5); Fe2−N7, 2.177(4); Fe2−N8, 2.142(4); Fe1−O−Fe2, 174.6(2); N3−Fe1−N4, 82.4(2); N3−Fe1−N1, 77.3(2); N6−Fe2−N7, 83.6(2); N6−Fe2−N5, 76.9(2).

systems have been studied for this activity, and it has been shown that copper(II) species must be reduced either chemically or electrochemically before a reaction with oxygen is observed.[25] Therefore, it is logical that the copper(II) species **5** did not show an interaction with dioxygen.

The desired reactivity for the series **1**−**5** is the catalytic four-electron reduction of oxygen to water. Any alternate pathway that is kinetically or thermodynamically favorable will greatly reduce the turnover of the catalyst, as well as generate undesirable side products that may interfere with the environment of the fuel cell. For this divalent series, only **2** appears to have a thermodynamic metal-oxo sink.

**Electrochemistry.** Given the eventual goal of employing complexes **1**−**5** as electrocatalysts, their electrochemical behavior was examined using cyclic voltammetry (CV) in acetonitrile with 0.1 M ($^n$Bu$_4$N)(PF$_6$) as the supporting electrolyte, and an Ag/Ag$^+$ reference (Figure 6). The CVs of the iron and copper complexes show reversible one-electron redox waves (Figure 6b and e). In contrast, the manganese, cobalt, and nickel complexes reveal more complicated electrochemical behavior (Figure 6a, c, and d).

The voltammogram of **1** shows an irreversible one-electron oxidation wave at 1.79 V ($E_{pa}$, Table 3). This wave is assigned to a metal-based $Mn^{3+}/Mn^{2+}$ oxidation. The process is irreversible even with increasing scan rate (Figure 6a),

**Table 3. Cyclic Voltammetry Data for Complexes 1−5**[a]

| complex | $E_{pc}$[b] | $E_{pa}$[c] | $E_{1/2}$[d] | redox couple |
|---|---|---|---|---|
| **1** | | 1.79 | | $Mn^{3+}/Mn^{2+}$ |
| **2** | 1.11 | 1.19 | 1.15 | $Fe^{3+}/Fe^{2+}$ |
| **3** | −1.15 | −1.03 | −1.09 | $Co^{2+}/Co^{1+}$ |
| **4** | −1.15 | −1.00 | −1.08 | $Ni^{2+}/Ni^{1+}$ |
| **5** | 0 | 0.06 | 0.03 | $Cu^{2+}/Cu^{1+}$ |

[a]Measurements taken under inert atmosphere in MeCN at 25 °C with 1 mM catalyst (5 mM of **1**) and 0.1 M ($^n$Bu$_4$N)(PF$_6$). [b]Cathodic peak potential (V vs Ag/Ag$^+$). [c]Anodic peak potential (V vs Ag/Ag$^+$). [d]Half-wave potential (V vs Ag/Ag$^+$).

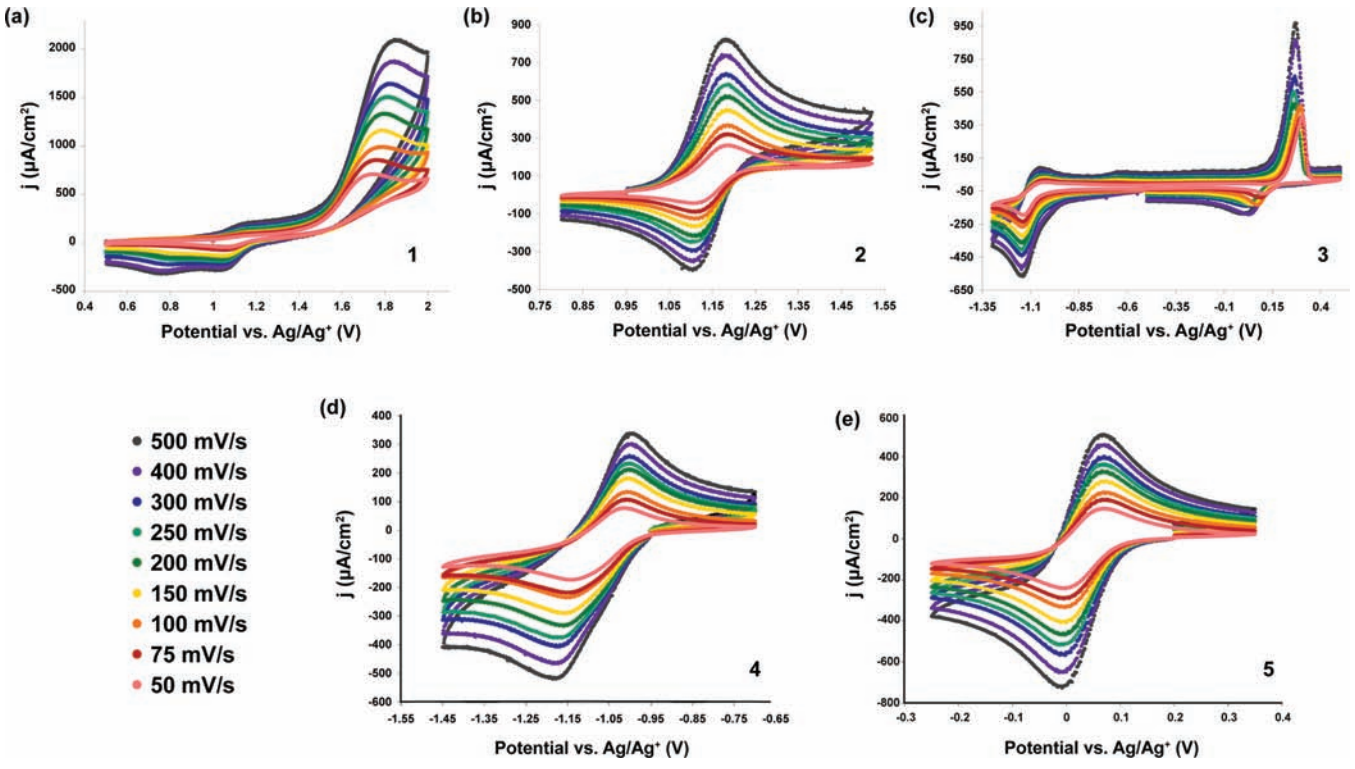


**Figure 6.** Variable scan rate cyclic votammagrams of complexes **1**−**5**, (a)−(e) respectively, with 1 mM catalyst (5 mM of **1** in a) in MeCN, 25 °C.


dx.doi.org/10.1021/ic2026957 | Inorg. Chem. 2012, 51, 4694−4706

indicating that the redox event is followed by an irreversible chemical reaction.

Characteristic of many iron(II) complexes, complex **2** displays a reversible one-electron oxidation at 1.15 V ($E_{1/2}$, Table 3). These waves are assigned to a reversible $Fe^{3+}/Fe^{2+}$ redox couple. The redox potential of **2** is significantly more positive (0.8 V or more) than that of similar iron TPA complexes.[81] This is likely due to the high-spin, low-spin nature of the complex in question, as a high-spin iron(II) complex is expected to be much easier to oxidize than a low-spin iron(II) complex.

Cobalt complex **3** displays unusual electrochemical behavior (Figure 6c). Oxygen reduction chemistry involving cobalt often employs a $Co^{2+}/Co^{3+}$ redox couple; however, these redox states are not observed in the solution CV. On the reductive side of the voltammogram, there is a quasi-reversible wave ($E_{1/2}$, Table 3) corresponding to a one-electron reduction. This is a metal-based reduction that is attributed to a $Co^{2+}/Co^{1+}$ couple. Interestingly, at low scan rates the wave is almost completely irreversible, but at faster scan rates, the wave approaches reversibility. This phenomenon has been observed with a bipyridyl cobalt system and is attributed to an EC (electrochemical/chemical) process that is only observed for certain scan rates in the CV.[82]

Cobalt(II) is reduced to cobalt(I), but on the time scale of the CV experiment a disproportionation occurs to give both $Co^0$ and $Co^{2+}$, leaving no $Co^{1+}$ in solution to be reoxidized back to $Co^{2+}$. The $Co^0$ is deposited as a black solid on the electrode surface. The adsorption-type oxidation peak seen around 300 mV is consistent with $Co^0$ being oxidized from the surface, and is absent if the potential is not initially swept in the reductive direction to the potential where the $Co^{2+}/Co^{1+}$ reduction occurs. At faster scan rates, some of the $Co^{1+}$ is oxidized to $Co^{2+}$ before disproportionation occurs, as is clearly seen by the growth of an oxidation peak at −1.03 V ($E_{pa}$, Table 3).

The CV of nickel derivative **4** displays only one major redox event that is quasi-reversible (Figure 6d). The half-wave potential of **4** has a value of −1.08 V ($E_{1/2}$, Table 3) and is assigned to a $Ni^{2+}/Ni^{1+}$ one-electron reduction. The peak-to-peak separation is too great to be considered a reversible process. This could possibly be due to the need for ligand exchange prior to reduction. From the solid-state structure presented previously, **4** is a 20-electron complex, and thus, it seems logical that decoordination of a solvent molecule may be required before an electron can be added.

Finally, the electrochemistry of copper complex **5** represents the other electrochemically reversible system of the series. As with iron(II), copper(II) complexes often display reversible $Cu^{2+}/Cu^{1+}$ redox couples. Complex **5** yields a redox potential of 0.03 V ($E_{1/2}$, Table 3) that corresponds to a reversible $Cu^{2+}/Cu^{1+}$ couple. This is comparable with other copper TPA dications reported in the literature, whose redox potentials reside around 0 V.[62,63]

Complexes **2** and **5** display fully reversible redox couples, while the remainder of the series demonstrate quasi-reversible or irreversible behavior. However, upon bubbling oxygen into the electrochemical cell, the CVs of the manganese, iron, cobalt, and copper derivatives changed dramatically. Complexes **1**−**3** and **5** displayed a loss of reversibility and an increase in current at the cathodic potential of the redox couple (see Supporting Information, Figures S1−S4). This behavior was absent under inert atmosphere, indicating a desired interaction of complexes **1**−**3** and **5** toward oxygen. As such, to rigorously determine the electrocatalytic oxygen reduction properties of the series, the compounds that showed an interaction with oxygen in solution were characterized further as oxygen-reduction electrocatalysts in a traditional manner.

**Electrocatalytic $O_2$ Reduction.** Complexes **1**−**3** and **5** were investigated by employing a commonly used approach for studying ORR electrocatalysts. Each compound was adsorbed on aerogel carbon powder, made into an ink with Nafion and deposited on a glassy carbon disk/platinum ring electrode. CVs were taken in acidic media (0.1 M $HClO_4$) under both inert and oxygen saturated atmospheres. In deoxygenated solutions, the redox behavior of **1**−**3** and **5** is electrochemically irreversible. All show one redox couple associated with the complex (for cyclic voltammograms, see Supporting Information, Figures S5−S8), which is at lower overpotentials when compared to those measured in solution ($E_{pc}$, Table 4). This disparity in redox potentials is attributed to the coordination environment of complexes **1**−**3** and **5** after adsorption, which is likely different from that observed in solution.[83] Moreover, when deposited on the surface, all four complexes showed no degradation or loss of activity during electrochemical measurements, making additional characterization possible.

**Table 4. Electrochemical Data for Adsorbed Complexes 1−3 and 5**[a]

| | | catalytic $O_2$ reduction | |
|---|---|---|---|
| complex | $E_{pc}$[b] | $*E_{pc}$[c] | % $H_2O_2$[d] |
| **1** | −0.02 | +0.38, +0.23, −0.07 | 20 |
| **2** | +0.15 | +0.13 | 11 |
| **3** | −0.02 | +0.37, +0.26 | 28 |
| **5** | +0.14 | +0.27, +0.09, −0.07 | 0 |

[a]Measurements taken in 0.1 M $HClO_4$ at 25 °C. [b]Cathodic peak potential under inert atmosphere (V vs RHE). [c]Cathodic peak potential in oxygen-saturated solution (V vs RHE). [d]ORR product yield ($H_2O$ vs $H_2O_2$) as calculated from the ring currents in Figure 6.

To determine the ORR activity of complexes **1**−**3** and **5** after adsorption, cyclic voltammograms were taken in the presence of oxygen. The curves display a significant increase in current density when compared to those conducted under inert atmosphere. This is attributed to catalytic oxygen reduction activity by the complexes, as the aerogel carbon has no ORR activity in this potential range.[84] Oxygen reduction occurs at multiple potentials for complexes **1**, **3**, and **5**, with each complex exhibiting multiple cathodic peaks ($*E_{pc}$, Table 4). For each of the four complexes, the $*E_{pc}$ with the lowest overpotential where oxygen reduction is observed does not have an associated oxidation peak. These observations are consistent with the reduction of the metal center, followed by subsequent electron transfer to an oxygen adduct of complexes **1**−**3** and **5**, reducing oxygen either via a two-electron reduction to peroxide or a four-electron reduction to water. The catalyst is chemically regenerated by reaction with oxygen, and thus, an anodic wave is not observed. Interestingly, the oxygen reduction onset potential, which is approximately 0.44 V for all complexes in the series investigated (Figure 6), does not seem to be drastically affected by the metal center present. This may indicate that the ligand has more of an affect over the potential where ORR occurs, as was also observed with metalloporhyrins, which show a dependence of the redox potential on the substituents on the ligand as a result of their electron withdrawing or donating properties.[85] However, this


dx.doi.org/10.1021/ic2026957 | Inorg. Chem. 2012, 51, 4694−4706

could also potentially be due to a kinetic limitation of the system, given the stark thermodynamic potential differences observed for **1**−**3** and **5** in solution (Figure 5).

Additionally, the propensity for two versus four-electron oxygen reduction, as catalyzed by **1**−**3** and **5**, was studied using rotating ring-disk electrode (RRDE) voltammetry. The RRDE voltammograms for complexes **1**−**3** and **5** (Figure 7) all display

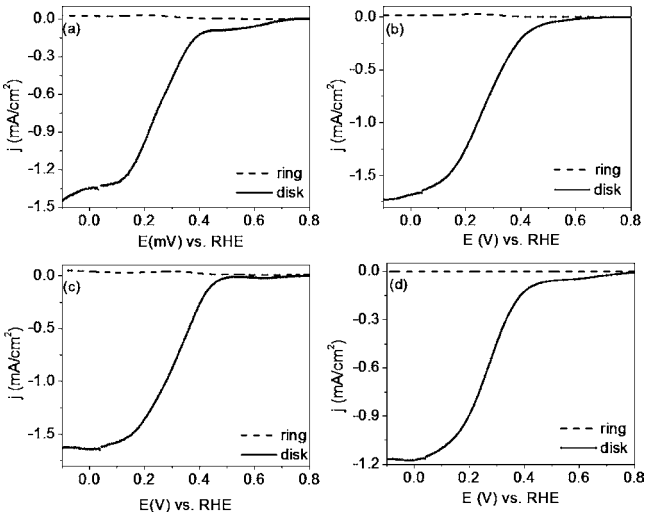


**Figure 7.** RRDE voltammograms for **1**−**3** and **5**, (a)−(d) respectively, in oxygen saturated 0.1 M $HClO_4$ at 1 mV/s and 400 rpm.

several disk waves. Although the onset potentials for oxygen reduction do not vary appreciably for **1**−**3** and **5**, the product yields ($H_2O$ vs $H_2O_2$) appear to be significantly affected by the metal center present (Table 4). While all four complexes display excellent selectivity for four-electron reduction, with **1**−**3** demonstrating 80, 89, and 72% conversion, respectively, the copper complex **5** exhibits complete conversion to water.

Finally, in order to determine the kinetic proficiencies of **1**−**3** and **5**, Koutecky−Levich plots (Figure 8) were constructed from the rotating disk voltammogram data.[86] Applying linear regression analysis to the data, the limiting current at infinite rotation speeds can be extrapolated from the *y*-intercept. The kinetic currents for **1**−**3** and **5** are 0.5, 7.6, 0.5, and 1.5 mA,

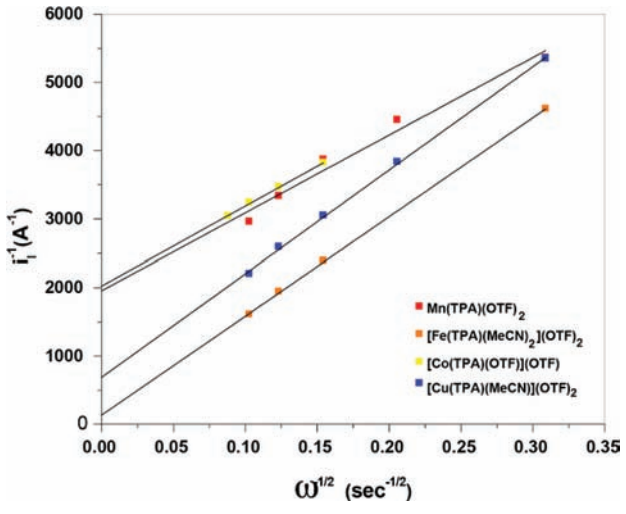


**Figure 8.** Koutecky−Levich plots of complexes **1**−**3** and **5**.

respectively, and are directly related to the heterogeneous rate constant for oxygen reduction. As with the onset potential for oxygen reduction, as well as the peroxide yield, the kinetics of **1**−**3** and **5** are comparable to those obtained under similar conditions for molecular species that have been employed as fuel cell catalysts.[87] While the oxygen reduction potential does not shift significantly between the complexes examined, as with the propensity for four-electron reduction, the kinetic efficiency of the catalyst does change with the metal center, with the iron complex **2** being the most kinetically active of the series. Given the great deal of literature precident concerning the mechanisms employed by various oxygen reduction catalysts, it is likely that the differences in ORR performance observed for **1**−**3** and **5** are linked both to the ability of each catalyst to employ bimetallic cooperativity and their mode of dioxygen binding. However, further electrochemical and characterization studies are necessary before direct structure function relationships can be difinitively asserted.

## ■ CONCLUSIONS

A series of simple first row catalysts $[(TPA)M^{2+}]^{n+}$ (M = Mn, Fe, Co, Ni, and Cu) have been prepared and characterized. Compounds **1**, **2**, **3**, and **5** were shown to electrocatalytically reduce dioxygen to water in a selective manner. All complexes showed onset potentials for ORR of roughly 0.44 V vs RHE, and displayed excellent selectivity for four-electron reduction over two-electron reduction (<28% $H_2O_2$), crucial for fuel cell applications. Additionally, the kinetic currents demonstrated by the complexes vary from 0.5 to 7.6 mA, respectively, with the iron complex **2** being the most active. These electrocatalytic properties are comparable to, and in some instances better than, current molecular catalysts in the literature. For the series presented, the metal center appears to dictate the peroxide yield and thus reaction kinetics, whereas the overpotential required to reduce oxygen seems to be influenced more strongly by the ligand. Future work will be aimed toward determining the specific mechanism of oxygen reduction for each catalyst, and applying this knowledge to both the selection of the most proficient metal center and the design of ligand systems capable of supporting catalysts that carry out ORR at potentials closer to the thermodynamic ideal.

## ■ EXPERIMENTAL SECTION

**General Procedures.** Unless otherwise noted, all reactions were performed using standard Schlenk line techniques or in an MBraun $N_2$-atmosphere glovebox (<1 ppm $O_2/H_2O$). All glassware, cannulae, and Celite were stored in an oven at ca. 150 °C. Diethyl ether, tetrahydrofuran, and dichloromethane were dried by passing over an activated alumina column and degassed with nitrogen prior to use.[88] Acetonitrile was distilled from $P_2O_5$ and degassed prior to use. *n*-Butanol was dried over 4 Å sieves and degassed prior to use. Deuterated solvents ($CD_3CN$ and $CDCl_3$) were vacuum-transferred from $CaH_2$ and degassed with three freeze−pump−thaw cycles. All NMR spectra were recorded at ambient temperature on Bruker AVQ-300, AVQ-400, or AVB-400 spectrometers. $^1H$ chemical shifts ($\delta$) are given relative to residual solvent peaks. $^{19}F$ chemical shifts ($\delta$) were referenced to an external standard ($CFCl_3$ at 0.00 ppm). Infrared (IR) spectra were recorded with a Thermo Scientific Nicolet iS10 FTIR spectrophotometer either as powder or as Nujol mulls between KBr plates. Magnetic susceptibility ($\mu_{eff}$) values were determined in $CD_3CN$ using the Evans' NMR method[68] at ambient temperature (25 °C). Electrical conductivity measurements were carried out in MeCN using a VWR sympHony meter, model SB80PC, with an Epoxy body Two Cell Platinum Conductivity Probe, model 11388-372. The cell constant was determined using a standard aqueous KCl


dx.doi.org/10.1021/ic2026957 | Inorg. Chem. 2012, 51, 4694−4706

solution. Conductivity measurements taken at various concentrations were used to construct Onsager plots of complexes **1**−**5** and were compared to standard 1:1 and 2:1 electrolytes.[62,89] Melting points were determined using sealed capillaries prepared under nitrogen and are uncorrected. Elemental analyses were determined at the Microanalytical Facility at the College of Chemistry, University of California, Berkeley. X-ray structural determinations were performed at CHEXRAY, University of California, Berkeley, on Bruker SMART 1000, SMART APEX, or MicroSTAR-H X8 APEXII diffractometers. The previously reported synthesis for tris(2-pyridylmethyl)amine[10] (TPA) did not yield consistent results, and an alternative procedure is given below. $[(TPA)Fe(MeCN)_2](OTf)_2$[49] was prepared by an alternative procedure given below. $(TPA)CoCl_2$ was made according to a previously reported literature procedure.[48] The remaining starting materials were obtained from commercial sources and used without further purification.

**Electrochemical Procedures.** Solution cyclic voltammograms were recorded with a Gamry Reference 600 potentiostat, using a glassy carbon working electrode (0.07 $cm^2$), a "no leak" silver/silver ion ($Ag/AgNO_3$) reference electrode calibrated to the ferrocinium/ferrocene redox couple (at 0.00 V), and a platinum counter electrode. Acetonitrile was used as the solvent with 0.1 M ($^nBu_4N$)($PF_6$) as supporting electrolyte. All solutions examined by CV were purged with nitrogen.

ORR electrochemical measurements were conducted using a Princeton Applied Research (PAR) VMP3 multi channel potentiostat and a Pine Instruments rotator. Two milligrams of complexes **1**−**3** and **5** were dissolved in 1 mL of water (18 MΩ·cm Millipore) combined with 1 $cm^2$ of aerogel carbon paper (Marketech International, Inc.), and allowed to adsorb on the carbon support for 24 h. The samples were then ground into a fine powder using a mortar and pestle. The powder was dissolved in 1 mL of DI water and sonicated for 30 min. Nafion (200 μL, 5% solution) was added to the catalyst ink and left to adsorb for 4 h. The ink (20 μL) was deposited on a glassy carbon disk (0.2475 $cm^2$) and allowed to air-dry. All experiments were conducted in 0.1 M $HClO_4$ using a rotating platinum ring—glassy carbon disk electrode (RRDE), a reversible hydrogen (RHE) reference electrode at 25 °C, and a glassy carbon counter electrode. Thin-film cyclic voltammograms were conducted first under an inert atmosphere and subsequently in oxygen-saturated solutions. RRDE experiments in oxygen-saturated solutions were conducted at a scan rate of 1 mV/s in order to minimize the columbic currents from the high surface area carbon support.

**Tris(2-pyridylmethyl)amine (TPA).** To a suspension of NaI (6.85 g, 0.046 mol) and $Cs_2CO_3$ (29.8 g, 0.091 mol) in 100 mL of MeCN was added 2-(chloromethyl)pyridine hydrochloride (5.0 g, 0.03 mol) to produce an orange suspension. To the reaction mixture was added 2-picolylamine (1.57 mL, 0.015 mol). The mixture was stirred vigorously for 48 h and monitored by TLC (9:1 DCM/MeOH, 1% $Et_3N$). The reaction mixture was filtered and the solids washed (3 × 100 mL) with MeCN to give an orange solution. The extracts were combined and the solvent removed in vacuo to yield a red solid. The solid was extracted with $Et_2O$ (3 × 25 mL) and chilled overnight at −40 °C to afford the product as colorless blocks (2.68 g, 61% yield).

**$(TPA)Mn(OTf)_2$ (1).** A solution of TPA (333 mg, 1.15 mmol) in 10 mL of MeCN was added to a solution of $Mn(OTf)_2$ (405 mg, 1.15 mmol) in 10 mL of MeCN to produce a pale yellow solution. After stirring at RT for 12 h, the reaction mixture was filtered to yield a yellow solution. The filtrate was concentrated until it became viscous, and $Et_2O$ was carefully layered on top to give colorless blocks via diffusion induced precipitation over 24 h (576 mg, 78% yield). Single crystals suitable for X-ray diffraction were obtained by slow diffusion of $Et_2O$ into **1** in MeCN. $^1H$ NMR (300 MHz, $CD_3CN$, 22 °C) δ 53.46 (br, s), 51.24 (br, s), 14.59 (br, s). $^{19}F$ NMR (400 MHz, $CD_3CN$, 22 °C) δ −52.80 (s, br, OTf). IR ($cm^{-1}$): 1609 (m), 1576 (w), 1484 (w), 1446 (s), 1317 (s), 1296 (m), 1243 (s), 1216 (s), 1166 (m), 1101 (w), 1055 (w), 1036 (s), 1020 (m), 907 (w), 800 (w), 768 (m), 760 (m), 723 (w), 636 (s). Anal. Calcd (%) for $C_{20}H_{18}F_6MnN_4O_6S_2$: C, 39.52; H, 3.32; N, 11.53. Found: C, 39.66; H, 3.46; N, 11.34. Mp = 174.2−174.8 °C. $\mu_{eff}$ = 5.9(1) $\mu_B$.

**$[(TPA)Fe(MeCN)_2](OTf)_2$ (2).** A solution of TPA (200 mg, 0.69 mmol) in 2 mL of MeCN was added to a suspension of $Fe(OTf)_2$ (244 mg, 0.69 mmol) in 5 mL of MeCN to produce a red suspension. After stirring at room temperature for 1 h, the reaction mixture was filtered to yield a red solution. $Et_2O$ was added to the filtrate to precipitate the previously reported compound as a red microcrystalline solid (440 mg, 88% yield). $^{19}F$ NMR (400 MHz, $CD_3CN$, 22 °C) δ −77.96 (s, OTf). IR ($cm^{-1}$): 1608 (m), 1574 (w), 1486 (w), 1467 (w), 1445 (m), 1262 (s), 1221 (s), 1153 (s), 1100 (m), 1026 (s), 908 (w), 818 (m), 763 (s), 735 (m). Mp (dec) = 90.9 °C.

**$[(TPA)Co(OTf)](OTf)$ (3).** A solution of $(TPA)CoCl_2$ (420 mg, 1.0 mmol) in 20 mL of MeCN was added via cannula to a suspension of Ag(OTf) (61 mg, 3.0 mmol) in 20 mL of MeCN to produce a pink-purple suspension. After stirring at room temperature for 15 min, the reaction mixture was filtered through Celite to yield a dark pink-purple solution. The filtrate was concentrated until it became viscous, and $Et_2O$ was carefully added until the product began to crystallize. The solution was then chilled overnight at −40 °C to afford the product as gray-purple needles (620 mg, 96% yield). Single crystals suitable for X-ray diffraction were obtained by vapor diffusion of $Et_2O$ into a concentrated solution of **3** in MeCN. $^1H$ NMR (300 MHz, $CD_3CN$, 22 °C) δ 161.40 (s), 72.36 (s), 63.08 (br, s), 57.04 (s), 6.33 (s). $^{19}F$ NMR (400 MHz, $CD_3CN$, 22 °C) δ −77.09 (s, OTf). IR ($cm^{-1}$): 1614 (m), 1574 (w), 1487 (w), 1446 (m), 1326 (m), 1302 (s), 1266 (m), 1208 (m), 1170 (m), 1106 (w), 1058 (w), 1029 (s), 1003 (w), 976 (w), 782 (w), 765 (m), 734 (w), 637 (m). Anal. Calcd (%) for $C_{20}H_{18}CoF_6N_4O_6S_2$: C, 37.10; H, 2.80; N, 8.65. Found: C, 36.76; H, 2.98; N, 8.37. Mp (dec) = 160.0 °C. $\mu_{eff}$ = 4.2(1) $\mu_B$.

**$[(TPA)Ni(MeCN)_2](OTf)_2$ (4).** A solution of TPA (50 mg, 0.17 mmol) in 3 mL of MeCN was added to a solution of $Ni(OTf)_2$ (61 mg, 0.17 mmol) in 3 mL of MeCN to produce a pale yellow suspension. After stirring at RT for 72 h, the reaction mixture was filtered to yield a pink solution. The filtrate was concentrated until it became viscous and $Et_2O$ was carefully layered on top to give pink-purple needles via diffusion induced precipitation over 24 h (108 mg, 87% yield). Single crystals suitable for X-ray diffraction were obtained by slow diffusion of $Et_2O$ into **4** in MeCN. $^1H$ NMR (300 MHz, $CD_3CN$, 22 °C) δ 53.46 (br, s), 51.24 (br, s), 14.59 (br, s). $^{19}F$ NMR (400 MHz, $CD_3CN$, 22 °C) δ −77.91 (s, OTf). IR ($cm^{-1}$): 2324 (w, CN), 2307 (w, CN), 2295 (w, CN), 2281 (w, CN), 1609 (m), 1259 (s), 1225 (m), 1144 (s), 1102 (w), 1056 (w), 1030 (s), 975 (w), 945 (w), 912 (w), 785 (m), 756 (m), 736 (w), 723 (w), 637 (s), 573 (m), 517 (m). Anal. Calcd (%) for $C_{24}H_{24}F_6N_6NiO_6S_2$: C, 39.52; H, 3.32; N, 11.53. Found: C, 39.66; H, 3.46; N, 11.34. Mp (dec) = 77.0 °C. $\mu_{eff}$ = 2.9(1) $\mu_B$.

**$[(TPA)Cu(MeCN)](OTf)_2\cdot(MeCN)$ (5).** A solution of TPA (300 mg, 1.0 mmol) in 10 mL of MeCN was added to a solution of $Cu(OTf)_2$ (374 mg, 1.0 mmol) in 10 mL of MeCN to produce a dark blue solution. After stirring at RT for 2 h, the reaction mixture was filtered and the filtrate was concentrated until it became viscous. $Et_2O$ was carefully layered on top to give blue hexagonal crystals via diffusion induced precipitation over 24 h (620 mg, 87% yield). Single crystals suitable for X-ray diffraction were obtained by slow diffusion of $Et_2O$ into **5** in MeCN. $^1H$ NMR (400 MHz, $CD_3CN$, 22 °C) δ 30.99 (br, s), 10.70 (br, s). $^{19}F$ NMR (400 MHz, $CD_3CN$, 22 °C) δ −78.25 (s, OTf). IR ($cm^{-1}$): 2330 (m, CN), 2299 (m, CN), 1609 (m), 1255 (s), 1221 (m), 1150 (s), 1195 (w), 1031 (s), 974 (w), 955 (w), 907 (w), 770 (m), 757 (w), 722 (w), 638 (s), 573 (m), 518 (m), 505 (w). Anal. Calcd (%) for $C_{24}H_{24}CuF_6N_6O_6S_2$: C, 39.26; H, 3.30; N, 11.45. Found: C, 39.20; H, 3.50; N, 11.15. Mp (dec) = 79.6 °C. $\mu_{eff}$ = 1.5(1) $\mu_B$.

**$[(TPA)_2Fe_2(\mu\text{-}O)(OTf)_2](OTf)_2$ (6).** Using a known volume bulb, $O_2$ (6.9 mL, 0.28 mmol) was introduced to a solution of **2** (138 mg, 0.19 mmol) in 10 mL of DCM, giving a yellow solution. After stirring at RT for 48 h, a pale orange precipitate had formed. Following filtration, the solid was dissolved in MeCN, the resulting solution was concentrated until viscous, and $Et_2O$ was carefully layered on top to give microcrystalline red blocks via diffusion induced precipitation over 24 h (40 mg, 66% yield). Single crystals suitable for X-ray diffraction were obtained by vapor diffusion of $Et_2O$ into **6** in MeCN. $^1H$ NMR


dx.doi.org/10.1021/ic2026957 | Inorg. Chem. 2012, 51, 4694−4706

(400 MHz, $CD_3CN$, 22 °C) $\delta$ 30.65 (br, s), 18.65 (br, s), 6.17 (br, s). $^{19}F$ NMR (400 MHz, $CD_3CN$, 22 °C) $\delta$ −74.22 (br, s, OTf). IR ($cm^{-1}$): 1609 (m), 1574 (w), 1488 (w), 1446 (w), 1325 (m), 1259 (s), 1235 (s), 1202 (s), 1154 (s), 1102 (m), 1059 (m), 1026 (s), 1010 (s), 908 (w), 817 (s), 764 (s), 725 (m). Anal. Calcd (%) for $C_{40}H_{36}F_{12}Fe_2N_8O_{13}S_4$: C, 36.82; H, 2.78; N, 8.59. Found: C, 37.10; H, 2.97; N, 8.34. Mp (dec) = 190.1 °C. $\mu_{eff}$ = 3.2(1) $\mu_B$.

**Crystallographic Analyses.** Single crystals of compounds **1** and **3**−**6** were coated in Paratone-N oil and mounted on a Kaptan loop. The loop was transferred to either a Bruker SMART 1000, SMART APEX, or MicroSTAR-H X8 APEXII diffractometer equipped with a CCD area detector,[90] centered in the beam, and cooled with an Oxford Cryostream 700 LT device that has been previously calibrated by a thermocouple placed at the same position as the crystal. Preliminary orientation matrixes and cell constants were determined by collection of 60, 30 s frames, followed by spot integration and least-squares refinement. An arbitrary hemisphere of data was collected, and the raw data were integrated using SAINT.[91] Cell dimensions reported were calculated from all reflections with $I > 10\sigma$. The data were corrected for Lorentz and polarization effects; no correction for crystal decay was applied. Data were analyzed for agreement and possible absorption using XPREP.[92] An empirical absorption correction based on comparison of redundant and equivalent reflections was applied using SADABS.[93] The structures were solved using SHELXS[94] and refined on all data by full-matrix least-squares with SHELXL-97.[95] Thermal parameters for all non-hydrogen atoms were refined anisotropically. ORTEP diagrams were created using ORTEP-3.[96] Compound **6** possessed highly disordered outer sphere acetonitrile molecules, and the data was treated with the SQUEEZE routine included in PLATON.[97]

## ■ ASSOCIATED CONTENT

### Ⓢ Supporting Information

Crystallographic data for complexes **1** and **3**−**6** (CIF), additional cyclic voltammograms, rotating disk voltammograms, and infrared spectra. This material is available free of charge via the Internet at http://pubs.acs.org.

## ■ AUTHOR INFORMATION

### Corresponding Author

*E-mail: arnold@berkeley.edu.

### Notes

The authors declare no competing financial interest.

## ■ ACKNOWLEDGMENTS

This work was supported by the Assistant Secretary for Energy Efficiency and Renewable Energy, Office Fuel Cell Technologies, of the U.S. Department of Energy under Contract No. DE-AC02-05CH11231. A.L.W. acknowledges the NSF for a predoctoral fellowship and the UCB Department of Chemistry for the Abramson Fellowship.

## ■ REFERENCES

(1) *Dioxygen Acivation and Homogeneous Catalytic Oxidation*; Simándi, L. I., Ed.; Elsevier Science Publishers B.V.: Amsterdam, 1991.
(2) Chen, K.; Costas, M.; Kim, J.; Tipton, A.; Que, L. *J. Am. Chem. Soc.* **2002**, *124*, 3026−3035.
(3) *Bioinorganic Catalysis*, 2nd ed.; Marcel Dekker: New York, 1999.
(4) Collman, J. P.; Ghosh, S. *Inorg. Chem.* **2010**, *49*, 5798−5810.
(5) Dawson, J. H. *Science* **1988**, *240*, 433−439.
(6) Kovaleva, E. G.; Lipscomb, J. D. *Nat. Chem. Biol.* **2008**, *4*, 186−193.
(7) Lee, Y.; Hong, S.; Morimoto, Y.; Shin, W.; Fukuzumi, S.; Nam, W. *J. Am. Chem. Soc.* **2010**, *132*, 10668−10670.
(8) *Biomimetic Oxidations Catalyzed by Transition Metal Complexes*; Meunier, B., Ed.; Imperial College Press: London, 2000.
(9) Mirica, L. M.; Vance, M.; Rudd, D. J.; Hedman, B.; Hodgson, K. O.; Solomon, E. I.; Stack, T. D. P. *Science* **2005**, *308*, 1890−1892.
(10) Tyeklar, Z.; Jacobson, R.; Wei, N.; Murthy, N.; Zubieta, J.; Karlin, K. *J. Am. Chem. Soc.* **1993**, *115*, 2677−2689.
(11) Steele, B. C. H.; Heinzel, A. *Nature* **2001**, *414*, 345−352.
(12) Gewirth, A. A.; Thorum, M. S. *Inorg. Chem.* **2010**, *49*, 3557−3566.
(13) Soukharev, V.; Mano, N.; Heller, A. *J. Am. Chem. Soc.* **2004**, *126*, 8368−8369.
(14) Savéant, J. *Chem. Rev.* **2008**, *108*, 2348−2378.
(15) Li, W.; Yu, A.; Higgins, D. C.; Llanos, B. G.; Chen, Z. *J. Am. Chem. Soc.* **2010**, *132*, 17056−17058.
(16) Matter, P. H.; Biddinger, E. J.; Ozkan, U. S. *Catalysis* **2007**, *20*, 338−361.
(17) Gasteiger, H.; Kocha, S.; Sompalli, B.; Wagner, F. *Appl. Catal., B* **2005**, *56*, 9−35.
(18) Stamenkovic, V. R.; Fowler, B.; Mun, B. S.; Wang, G. F.; Ross, P. N.; Lucas, C. A.; Markovic, N. M. *Science* **2007**, *315*, 493−497.
(19) Wang, B. *J. Power Sources* **2005**, *152*, 1−15.
(20) Ye, H. C.; Crooks, R. M. *J. Am. Chem. Soc.* **2007**, *129*, 3627−3633.
(21) McCrory, C. C. L.; Devadoss, A.; Ottenwaelder, X.; Lowe, R. D.; Stack, T. D. P.; Chidsey, C. E. D. *J. Am. Chem. Soc.* **2011**, *133*, 3696−3699.
(22) Thorum, M. S.; Yadav, J.; Gewirth, A. A. *Angew. Chem., Int. Ed.* **2009**, *48*, 165−167.
(23) Chang, C. J.; Loh, Z. H.; Shi, C. N.; Anson, F. C.; Nocera, D. G. *J. Am. Chem. Soc.* **2004**, *126*, 10013−10020.
(24) Dogutan, D. K.; Stoian, S. A.; McGuire, R.; Schwalbe, M.; Teets, T. S.; Nocera, D. G. *J. Am. Chem. Soc.* **2011**, *133*, 131−140.
(25) Fukuzumi, S.; Kotani, H.; Lucas, H. R.; Doi, K.; Suenobu, T.; Peterson, R. L.; Karlin, K. D. *J. Am. Chem. Soc.* **2010**, *132*, 6874−6875.
(26) Chang, C. J.; Deng, Y. Q.; Shi, C. N.; Chang, C. K.; Anson, F. C.; Nocera, D. G. *Chem. Commun.* **2000**, 1355−1356.
(27) Shook, R. L.; Peterson, S. M.; Greaves, J.; Moore, C.; Rheingold, A. L.; Borovik, A. S. *J. Am. Chem. Soc.* **2011**, *133*, 5810−5817.
(28) Yang, J. Y.; Bullock, R. M.; Dougherty, W. G.; Kassel, W. S.; Twamley, B.; DuBois, D. L.; DuBois, M. R. *Dalton Trans.* **2010**, *39*, 3001−3010.
(29) Karlin, K.; Kaderli, S.; Zuberbuhler, A. *Acc. Chem. Res.* **1997**, *30*, 139−147.
(30) Jacobson, R.; Tyeklar, Z.; Farooq, A.; Karlin, K.; Liu, S.; Zubieta, J. *J. Am. Chem. Soc.* **1988**, *110*, 3690−3692.
(31) Cracknell, J. A.; Vincent, K. A.; Armstrong, F. A. *Chem. Rev.* **2008**, *108*, 2439−2461.
(32) Karlin, K.; Hayes, J.; Juen, S.; Hutchinson, J.; Zubieta, J. *Inorg. Chem.* **1982**, *21*, 4106−4108.
(33) Thallaj, N. K.; Rotthaus, O.; Benhamou, L.; Humbert, N.; Elhabiri, M.; Lachkar, M.; Welter, R.; Albrecht-Gary, A.-M.; Mandon, D. *Chem.—Eur. J.* **2008**, *14*, 6742−6753.
(34) Suzuki, M. *Acc. Chem. Res.* **2007**, *40*, 609−617.
(35) Beni, A.; Dei, A.; Laschi, S.; Rizzitano, M.; Sorace, L. *Chem.—Eur. J.* **2008**, *14*, 1804−1813.
(36) Grubel, K.; Fuller, A. L.; Chambers, B. M.; Arif, A. M.; Berreau, L. M. *Inorg. Chem.* **2010**, *49*, 1071−1081.
(37) Dong, Y.; Fujii, H.; Hendrich, M.; Leising, R.; Pan, G.; Randall, C.; Wilkinson, E.; Zang, Y.; Que, L.; Fox, B.; Kauffmann, K.; Münck, E. *J. Am. Chem. Soc.* **1995**, *117*, 2778−2792.
(38) Kaizer, J.; Klinker, E. J.; Oh, N. Y.; Rohde, J. U.; Song, W. J.; Stubna, A.; Kim, J.; Münck, E.; Nam, W.; Que, L. *J. Am. Chem. Soc.* **2004**, *126*, 472−473.
(39) Fry, H.; Scaltrito, D.; Karlin, K.; Meyer, G. *J. Am. Chem. Soc.* **2003**, *125*, 11866−11871.
(40) Jang, H.; Cox, D.; Que, L. *J. Am. Chem. Soc.* **1991**, *113*, 9200−9204.
(41) McCrory, C. C. L.; Devadoss, A.; Ottenwaelder, X.; Lowe, R. D.; Stack, T. D. P.; Chidsey, C. E. D. *J. Am. Chem. Soc.* **2011**, *133*, 3696−3699.

(42) Thorseth, M. A.; Letko, C. S.; Rauchfuss, T. B.; Gewirth, A. A. *Inorg. Chem.* **2011**, *50*, 6158−6162.
(43) Coperet, C.; Chabanas, M.; Saint-Arroman, R. P.; Basset, J. M. *Angew. Chem., Int. Ed.* **2003**, *42*, 156−181.
(44) Koper, M. T. M.; Bouwman, E. *Angew. Chem., Int. Ed.* **2010**, *49*, 3723−3725.
(45) Chen, K.; Que, L. *J. Am. Chem. Soc.* **2001**, *123*, 6327−6337.
(46) Fernicola, A.; Weise, F. C.; Greenbaum, S. G.; Kagimoto, J.; Scrosati, B.; Soleto, A. *J. Electrochem. Soc.* **2009**, *156*, A514−A520.
(47) Alcock, H. J.; White, O. C.; Jegelevicius, G.; Roberts, M. R.; Owen, J. R. *J. Power Sources* **2011**, *196*, 3355−3359.
(48) Davies, C.; Solan, G.; Fawcett, J. *Polyhedron* **2004**, *23*, 3105−3114.
(49) Diebold, A.; Hagen, K. *Inorg. Chem.* **1998**, *37*, 215−223.
(50) Goodson, P.; Oki, A.; Glerup, J.; Hodgson, D. *J. Am. Chem. Soc.* **1990**, *112*, 6248−6254.
(51) Hitomi, Y.; Ando, A.; Matsui, H.; Ito, T.; Tanaka, T.; Ogo, S.; Funabiki, T. *Inorg. Chem.* **2005**, *44*, 3473−3478.
(52) Shin, B.; Kim, Y.; Kim, M.; Han, J. *Polyhedron* **2007**, *26*, 4557−4566.
(53) Chin, D.; Delgaudio, J.; Lamar, G.; Balch, A. *J. Am. Chem. Soc.* **1977**, *99*, 5486−5488.
(54) Kadish, K.; Frémond, L.; Ou, Z.; Shao, J.; Shi, C.; Anson, F.; Burdet, F.; Gros, C.; Barbe, J.; Guilard, R. *J. Am. Chem. Soc.* **2005**, *127*, 5625−5631.
(55) Addison, A. W.; Rao, T. W.; Reedijk, J.; Rijn, J.; Verschoor, C. G. *J. Chem. Soc., Dalton Trans.* **1984**, *7*, 1349−1356.
(56) Min, K. S.; DiPasquale, A. G.; Golen, J. A.; Rheingold, A. L.; Miller, J. S. *J. Am. Chem. Soc.* **2007**, *129*, 2360−2368.
(57) Massoud, S. S.; Broussard, K. T.; Mautner, F. A.; Vicente, R.; Saha, M. K.; Bernal, I. *Inorg. Chim. Acta* **2008**, *361*, 123−131.
(58) Wilkinson, G.; Pauson, P. L.; Cotton, F. A. *J. Am. Chem. Soc.* **1954**, *76*, 1970−1974.
(59) Szajna, E.; Dobrowolski, P.; Fuller, A.; Arif, A.; Berreau, L. *Inorg. Chem.* **2004**, *43*, 3988−3997.
(60) Tano, T.; Doi, Y.; Inosako, M.; Kunishita, A.; Kubo, M.; Ishimaru, H.; Ogura, T.; Sugimoto, H.; Itoh, S. *Bull. Chem. Soc. Jpn.* **2010**, *83*, 530−538.
(61) Inosako, M.; Kunishita, A.; Kubo, M.; Ogura, T.; Sugimoto, H.; Itoh, S. *Dalton Trans.* **2009**, 9410−9417.
(62) Zhang, C.; Kaderli, S.; Costas, M.; Kim, E.; Neuhold, Y.; Karlin, K.; Züberbuhler, A. *Inorg. Chem.* **2003**, *42*, 1807−1824.
(63) Chuang, C.; Lim, K.; Chen, Q.; Zubieta, J.; Canary, J. *Inorg. Chem.* **1995**, *34*, 2562−2568.
(64) Lim, B. S.; Holm, R. H. *Inorg. Chem.* **1998**, *37*, 4898−4908.
(65) Shannon, R. D. *Acta Crystallogr., Sect. A: Found. Crystallogr.* **1976**, *32*, 751−767.
(66) Ito, M.; Sakai, K.; Tsubomura, T.; Takita, Y. *Bull. Chem. Soc. Jpn.* **1999**, *72*, 239−247.
(67) Makowska-Grzyska, M.; Szajna, E.; Shipley, C.; Arif, A.; Mitchell, M.; Halfen, J.; Berreau, L. *Inorg. Chem.* **2003**, *42*, 7472−7488.
(68) Piguet, C. *J. Chem. Educ.* **1997**, *74*, 815−816.
(69) Rozenel, S. S.; Kerr, J. B.; Arnold, J. *Dalton Trans.* **2011**, *40*, 10397−10405.
(70) Shafter, J.; Raymond, K. *Inorg. Chem.* **1971**, *10*, 1799−1803.
(71) Lee, D.; Wei, N.; Murthy, N. N.; Tyeklar, Z.; Karlin, K. D.; Kaderli, S.; Jung, B.; Zuberbuehler, A. D. *J. Am. Chem. Soc.* **1995**, *117*, 12498−12513.
(72) Blakesley, D.; Payne, S.; Hagen, K. *Inorg. Chem.* **2000**, *39*, 1979−1989.
(73) Borzel, H.; Comba, P.; Hagen, K.; Lampeka, Y.; Lienke, A.; Linti, G.; Merz, M.; Pritzkow, H.; Tsymbal, L. *Inorg. Chim. Acta* **2002**, *337*, 407−419.
(74) Fawcett, W.; Liu, G.; Kessler, T. *J. Phys. Chem.* **1993**, *97*, 9293−9298.
(75) Lippincott, E. R.; Welsh, F. E.; Weir, C. E. *Anal. Chem.* **1961**, *33*, 137−143.
(76) Pecoraro, V.; Baldwin, M.; Gelasco, A. *Chem. Rev.* **1994**, *94*, 807−826.
(77) Vanatta, R.; Strouse, C.; Hanson, L.; Valentine, J. *J. Am. Chem. Soc.* **1987**, *109*, 1425−1434.
(78) Kitajima, N.; Komatsuzaki, H.; Hikichi, S.; Osawa, M.; Morooka, Y. *J. Am. Chem. Soc.* **1994**, *116*, 11596−11597.
(79) Kurtz, D. M. Jr. *Chem. Rev.* **1990**, *90*, 585−606.
(80) Kieber-Emmons, M. T.; Riordan, C. G. *Acc. Chem. Res.* **2007**, *40*, 618−625.
(81) Benhamou, L.; Lachkar, M.; Mandon, D.; Welter, R. *Dalton Trans.* **2008**, *48*, 6996−7003.
(82) Buriez, O.; Cannes, C.; Nédélec, J.; Périchon, J. *J. Electroanal. Chem.* **2000**, *495*, 57−61.
(83) There is literature precedent for the coordination environment and the oxidation state of similar TPA complexes in the presence of both water and acid, and the metal-based redox states most often involved in oxygen reduction are known. These factors, in combination with the redox states observed in nonaqueous solution, make it likely that the complexes are operating as $M^{3+}/M^{2+}$ (**1**-**3**) and $M^{2+}/M^{+}$ (**5**) redox couples, with the coordination environment possibly involving metal-oxo dimers. However, further experiments are needed to confirm the exact nature of the complexes after adsorption. See refs 51 and (a) Korendovych, I.; Kryatov, S.; Reiff, W.; Rybak-Akimova, E. *Inorg. Chem.* **2005**, *44*, 8656−8658. (b) Sasaki, Y.; Kobayashi, T.; Masuda, H.; Einaga, H.; Ohba, S.; Nishida, Y. *Inorg. Chem. Commun.* **1999**, *2*, 244−246. (c) Kadish, K. M.; Smith, K. M.; Guilard, R. *The porphyrin handbook*; Academic Press: San Diego, 2000.
(84) Elbaz, L.; Korin, E.; Soifer, L.; Bettelheim, A. *J. Electroanal. Chem.* **2008**, *621*, 91−96.
(85) Elbaz, L.; Korin, E.; Soifer, L.; Bettelheim, A. *J. Electrochem. Soc.* **2010**, *157*, B27−B31.
(86) Koutecky−Levich plots (Figure 8) were constructed from the rotating disk voltammogram data (Figures S9-S12) according to the following equation:

$$1/iL = 1/i_{Lev} + 1/i_k$$

where $i_{Lev}$ is the Levich current given by:

$$i_{Lev} = 0.62nFAD^{2/3}\omega^{1/2}\nu^{-1/6}C_{O2}^{*}$$

and $i_k$ is the kinetic current defined by:

$$ik = nFAk\Gamma C_{O2}^{*}$$

where $A$ is the electrode area $cm^2$, $D$ and $C$ are the oxygen diffusion coefficient $cm^2\ s^{-1}$ and bulk concentration mol $L^{-1}$, respectively, $\nu$ is the kinematic viscosity of the solution $cm^2\ s^{-1}$, $\omega$ is the angular frequency of rotation ($\omega = 2\pi f/60$, f is the disk rotation rate rpm), $k$ is the rate constant $M^{-1}\ s^{-1}$ governing the reaction of the catalyst with oxygen, and $\Gamma$ is the surface coverage mol $cm^{-2}$ of the catalyst.
(87) Bettelheim, A.; White, B.; Murray, R. *J. Electroanal. Chem.* **1987**, *217*, 271−286.
(88) Alaimo, P. J.; Peters, D. W.; Arnold, J.; Bergman, R. G. *J. Chem. Educ.* **2001**, *78*, 64.
(89) Geary, W. *Coord. Chem. Rev.* **1971**, *7*, 81−122.
(90) *SMART: Area-Detector Software Package*, Bruker Analytical X-ray Systems, Inc., Madison, WI, 2001−2003.
(91) *SAINT: SAX Area-Detector Integration Program, V6.40*, Bruker Analytical X-ray Systems, Inc., Madison, WI, 2003.
(92) *PREP (v 6.12): Part of the SHELXTL Crystal Structure Determination Package*, Bruker Analytical X-ray Systems, Inc., Madison, WI, 2003.
(93) *SADABS: Bruker-Nonius Area Detector Scaling and Absorption, V2.05*, Bruker Analytical X-ray Systems, Inc., Madison, WI, 2003.
(94) *SHELXS: Program for the Refinement of X-ray Crystal Structures, Part of the SHELXTL Crystal Structure Determination Package*, Bruker Analytical X-ray Systems, Inc., Madison, WI, 1995−1999.
(95) *SHELXL: Program for the Refinement of X-ray Crystal Structures, Part of the SHELXT Crystal Structure Determination Package*, Bruker Analytical X-ray Systems, Inc., Madison, WI, 1997.
(96) Farrugia, L. *J. Appl. Crystallogr.* **1997**, *30*, 565.

(97) Spek, A. L. *PLATON—A Multipurpose Crystallographic Tool*, Utrecht University, Utrecht, The Netherlands, 2007.